Journal of Magnetism and Magnetic Materials 453 (2018) 36–43

Contents lists available at ScienceDirect

Journal of Magnetism and Magnetic Materials

journal homepage: www.elsevier.com/locate/jmmm

Research articles

Effect of Al-doped $YCrO_3$ on structural, electronic and magnetic properties

A. Durán [a,*], E. Verdín [b], A. Conde [c], R. Escamilla [d]

[a] Universidad Nacional Autónoma de México, Centro de Nanociencias y Nanotecnología, Km. 107 Carretera Tijuana-Ensenada, Apartado Postal 14, C. P. 22800, Ensenada, B.C., Mexico
[b] Universidad de Sonora, Departamento de Física, Apartado Postal 1626, Hermosillo, Sonora, Mexico
[c] Departamento de Física, CINVESTAV-IPN, Apartado Postal 14-740, México D.F. 07360, Mexico
[d] Universidad Nacional Autónoma de México, Instituto de Investigaciones en Materiales, Apartado Postal 70-360, México D.F. 04510, Mexico

ARTICLE INFO

Article history:
Received 6 October 2017
Received in revised form 30 November 2017
Accepted 31 December 2017
Available online 4 January 2018

Keywords:
Structure
Magnetism
Dielectric properties
Electrical conductivity

ABSTRACT

Structural, dielectric and magnetic properties were investigated in the $YCr_{1-x}Al_xO_3$ with $0 < x < 0.5$ compositions. XRD and XPS studies show that the partial substitution of the Al^{3+} ion decreases the cell volume of the orthorhombic structure without changes in the oxidation state of the Cr^{3+} ions. We discuss two mechanisms that could have a significant influence on the magnetic properties. The first is related to local deformation occurring for $x < 0.1$ of Al content and the second is related to change of the electronic structure. The local deformation is controlled by the inclination of the octahedrons and the octahedral distortion having a strong effect on the T_N and the coercive field at low Al concentrations. On the other hand, the decreasing of the magnetization values (M_r and H_c) is ascribed to changes in the electronic structure, which is confirmed by a decreasing of the contribution of Cr 3d states at Fermi level due to increasing Al^{3+} content. Thus, we analyzed and discussed that both mechanisms influence the electronic properties of the $YCr_{1-x}Al_xO_3$ solid solution.

1. Introduction

In recent years, a significant amount of research has been conducted in the orthochromite family due to their interesting magnetic and transport properties. In the past decades, their high thermic stability along with the excellent electrical conductivity in a wide range of temperature was attractive for a solid oxide fuel cell (SOFCs) applications, high-temperature electrode, and thermoelectric materials [1–3]. In recent years, the investigation has focused on the multiferroic properties since some members of this family present the coexistence or coupling between ferroelectric and magnetic properties [4–6]. The cross-coupled effect allows electric field control with potential impact in the spintronic and data storage high –frequency magnetic devices [7–9]. The orthochromite family are isostructural and crystallize in the orthorhombically distorted perovskite structure with centrosymmetric *Pbnm* space group. Although the space group is incompatible with traditional ferroelectric materials, the $YCrO_3$ has been reported with biferroic properties; i.e., the magnetic and ferroelectric transition occur at 140 and 473 K, respectively [5,10]. It is well known that the G-type antiferromagnetic structure arises from the Cr^{3+} (d^3) sublattice. The magnetic configuration, according to Bertaut notation [11] is Γ_4 (G_x, A_y, F_z) for $YCrO_3$. Below of T_N, the spin configuration remains weakly ferromagnetic due to antisymmetric Dzyaloshinski-Moriya (DM) interaction. In orthochromite family, the Cr–O–Cr angle tune the T_N when Y is substituted by rare earth ions [12]. It has also been found that the polar behavior can be reached through chemical pressure via B cation substitution in the perovskite structure, as it has been found in $YCr_{1-x}M_xO_3$ (M = Fe or Mn) compound [13]. The cationic substitution at the A and B sites in the perovskite structure has proved to be an effective alternative to induce new phenomena or to improve the magnetic and transport properties [14–17].

Other interesting features may occur in these materials, if, instead of substitutions of partially filled 3*d* orbitals, the Cr^{3+} is substituted by the fully 3d orbitals ions as, for example, Al^{3+} ions. Significant changes in transport properties should be expected since $YAlO_3$ is an insulating material with an experimental energy gap of 7.1 eV [18]. The replacement of the Cr^{3+} by Al^{3+} produce a complete solubility without a change in the orthorhombic *Pbnm* space group. The Cr^{3+} ions is a transition metal with partially filled *3d* orbitals and strong crystal field stabilization energy at the octahedral site, whereas Al^{3+} has full *3d* orbitals and thus exhibits no crystal field effects. Furthermore, such a substitution can enhance the hybridization between the internal states and so affect the

* Corresponding author.
E-mail address: dural@cnyn.unam.mx (A. Durán).

https://doi.org/10.1016/j.jmmm.2017.12.106
0304-8853/

structural, electronic and magnetic properties. From the magnetic and transport point of view, the $YCr_{1-x}Al_xO_3$ ceramic compounds have not been investigated.

Crystal structure, electronic and magnetic properties were studied in $YCr_{1-x}Al_xO_3$. XRD and XPS analysis confirm the high-quality samples obtained using the combustion method. The Al substitution has notable effects on the electric and magnetic properties. Here, we found that not only the changes in the electronic structure by the Al substitution affect the transport properties, but also the geometrical deformation has important effects on the magnetic parameters. These results are analyzed and discussed in this work.

2. Experimental details

Powder samples of $YCr_{1-x}Al_xO_3$ (YCAO) with x = 0.000, 0.025, 0.050, 0.075, 0.100, 0.200, 0.300 and 0.500 compositions were synthesized by combustion method. Stoichiometric quantities of Y_2O_3 (Sigma-Aldrich 99.99%), $Cr(NO_3)_3{\cdot}6H_2O$ (99.0%) and $Al(NO_3)_3{\cdot}9H_2O$ (Alfa-Aesar 98%) were weighted. The stoichiometric Y_2O_3 powder was dissolved in aqueous solution of 1:1 HNO_3 (Sigma-Aldrich 70%). Once the powders of Y_2O_3 are dissolved, the nitrate salts are added until the mixture was completely dissolved. The final solution containing the metallic ions was concentrated (by evaporation) and diluted (adding deionized water) several times until complete removal of HNO_3 in excess. Then, the cationic solution was mixed with glycine (Sigma-Aldrich 98.5%), stirred and heated at 170 °C to start the ignition process (1.5 g of glycine by 1 g of YCAO). Finally, the dried gel burnt in a self-propagating combustion manner to form loose combustion powder. The as-combustion powders were heated at a rate of 5 °C.min^{-1} to reach 1250 °C for 6 h in air. Phase identification in the samples was carried out with a Siemens D5000 X-ray (XRD) diffractometer using Co-K_α radiation and Fe filter. The powder X-ray diffraction patterns were measured in steps of 0.02° for 14 s in the 2θ range of 10° to 120° at room temperature. The crystallographic phases were identified using the JCPDS database. The crystallographic parameters were refined using the QUANTO program with multi-phase capability [19]. X-ray photoelectron spectroscopy analysis was performed in an ultra-high vacuum (UHV) system Scanning XPS microprobe PHI 5000 Versa Probe II, with an Al K_α X-ray source (hν = 1486.6 eV), and an MCD analyzer. The surface of the samples was etched for 2 min with 3.0 kV Ar^+ at 0.04 μA mm^{-2}. The XPS spectra were obtained at 45° to the normal surface in constant pass energy mode (CAE), E_0 = 100 and 10 eV for survey surface and high-resolution narrow scan, respectively. The peak positions were referenced to the C 1s hydrocarbon groups at 285.00 eV central peak core level position.

The $YCr_{1-x}Al_xO_3$ calcined powder was compacted in a cylindrical die with a diameter of 6 mm. Then, the sample was sintered as follows: green pellets were placed in alumina (99.9%) plate crucibles and heated at a rate of 5 °C.min^{-1} to 1680 K and kept there for 4 h and then cooled to room temperature. To evaluate the dielectric properties, the sintered pellets (6 × 1.2 mm) were finally coated with conductive silver paint, dried at 500 C for 1 min and cooled down to room temperature. The electric features of the samples were measured with an LCR (HP 4284 A) bridge from 1 kHz to 50 kHz. Magnetic measurements were performed using a Dynacool-PPMS system by Quantum Design.

3. Result and discussion

Fig. 1 (Upper panel) shows the X-ray diffraction patterns for the $Y(Cr_{1-x}Al_x)O_3$ with $0.000 \leq x \leq 0.300$ compositions. All diffraction peaks were completely indexed to an orthorhombic cell (JCPDS n° 34-0365) with space group *Pbnm*. Aluminum substitution brings

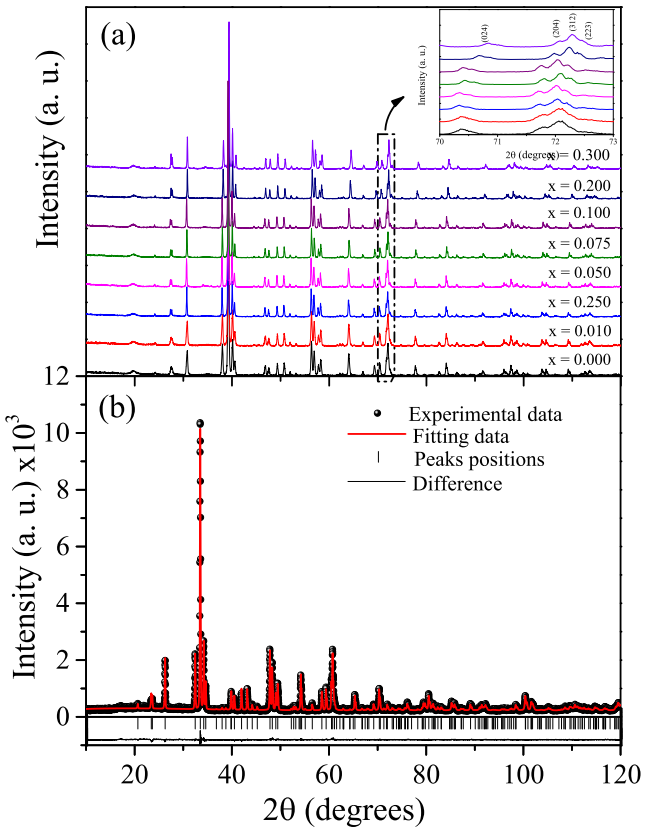

Fig. 1. (a) X-ray diffraction patterns for the $YCr_{1-x}Al_xO_3$ with 0 < x < 0.3 compositions. The inset shows the shift of the plane (024), (204), (312) and (223) as Al content. (b) $YCr_{0.8}Al_{0.2}O_3$ sample refined by Rietveld analysis at room temperature.

remarkable changes in the position of the diffraction peaks shifting to higher angles as seen in the inset of Fig. 1. The X-ray diffraction patterns were Rietveld-fitted considering the possibility that Al ions can occupy Cr^{3+} ions sites. Thus, the XRD calculated patterns matched satisfactorily with the experimental patterns in a whole range of Al substitution. As an example, we show in Fig. 1 (bottom panel) the fitted X-ray diffraction pattern for the $YCr_{0.8}Al_{0.2}O_3$ compound. Crystallographic data from the final refinement as well as the corresponding set of the R reliability factors are presented in Table 1. The lattice parameters, and the unit cell volume as a function of Al content (x) is shown Fig. 2. The lattice parameters obtained for the undoped sample are in agreement with other published results [5,6,20]. As can be seen, the lattice parameters decrease systematically with increasing the Al content; as a result, the unit cell volume decreases. This result might be explained considering the difference of the ionic radii between Cr^{3+} (0.615 Å) and Al^{3+} (0.535 Å) ions [21]. Note that the lattice parameters behavior is consistent under the criterion of chemical pressure effect, where the Al substitution produce an isotropic compressive effect in the $YCr_{1-x}Al_xO_3$ crystal. Selected bond lengths and bond angles are listed in Table 2. Each Cr^{3+}/Al^{3+} atom is coordinated by six oxygen atoms with three pairs of different bond distances. The apical bond lengths (Cr–O1) are shorter with symmetrical distance than the equatorial (Cr–O2) bond lengths. Upon Al^{3+} substitution, the net result is a decreasing of the average ⟨Cr–O⟩ bond length and an increase in the octahedral distortion (Δ). The Δ was obtained according to Ref. [22]. These effects on the structure are expected due to the difference of ionic radii between Cr^{3+}/Al^{3+} in the octahedral environment. Furthermore, the octahedral tiltings can be calculated using the expressions $\theta = (180 - \langle Cr{-}O(1){-}Cr\rangle)/2$ and $\cos\varphi = \cos((180 - \langle Cr{-}O(2){-}Cr\rangle)/2/\sqrt{\cos\theta}$ [Ref. 23]. However,

Table 1
Structural parameters and atomic positions for $YCr_{1-x}Al_xO_3$ system at room temperature.

x =		0.00	0.010	0.025	0.050	0.075	0.100	0.200	0.300
a (Å)		5.5255(3)	5.5264(1)	5.5224(1)	5.5173(3)	5.5132(1)	5.5070(1)	5.4912(2)	5.4735(2)
b (Å)		7.5384(3)	7.5402(1)	7.5356(1)	7.5295(2)	7.5265(1)	7.5202 (1)	7.5061(2)	7.4898(3)
c (Å)		5.2455(2)	5.2473(2)	5.2447(1)	5.2420(3)	5.2415(2)	5.2384(2)	5.2340 (3)	5.2279(3)
V (Å^3)		218.49	218.66	218.26	217.77	217.50	216.94	215.73	214.32
Y	x	0.0654(3)	0.0654(3)	0.0653(3)	0.0653(4)	0.0653(3)	0.0652(4)	0.0652(2)	0.0651(2)
	z	0.9835(1)	0.9835(1)	0.9836(1)	0.9836(2)	0.9836(1)	0.9837(2)	0.9837(2)	0.9838(2)
	B (Å^2)	0.20(3)	0.20(3)	0.31(4)	0.37(4)	0.36(3)	0.47(3)	0.31(4)	0.39(5)
Cr/Al	B (Å^2)	0.26(3)	0.28 (3)	0.22(3)	0.36(3)	0.29(3)	0.26(5)	0.36(3)	0.46(3)
O(1)	x	0.466(2)	0.466(2)	0.467(2)	0.467(1)	0.467(2)	0.468(2)	0.468(2)	0.469(2)
	z	0.093(1)	0.093(1)	0.093(2)	0.092(2)	0.092(1)	0.092(2)	0.091(1)	0.091(1)
	B (Å^2)	1.24(3)	1.24(3)	1.20(3)	1.46(3)	1.70(2)	1.64(1)	1.46(3)	1.20(3)
O(2)	x	0.284(1)	0.284(1)	0.284(2)	0.284(1)	0.285(1)	0.285(2)	0.286(1)	0.286(2)
	y	0.052(1)	0.052(1)	0.051(3)	0.051(1)	0.050(1)	0.050(2)	0.049(1)	0.049(2)
	z	0.311(1)	0.311(1)	0.312(1)	0.312(1)	0.313(1)	0.313(1)	0.314(1)	0.314(1)
	B (Å^2)	1.30(2)	1.30(2)	1.20(3)	1.35(2)	1.24(5)	1.39(5)	1.51(3)	1.29(5)
	R_b (%)	6.9	13.2	12.2	12.2	12.6	12.4	12.3	13.7
	R_{wp} (%)	9.3	18.5	17.8	17.8	18.6	18.6	18.4	20.0
	R_{exp} (%)	5.3	11.7|	10.9	10.9	10.7	11.2	11.5	10.5
	χ^2 (%)	1.8	1.6	1.6	1.6	1.7	1.7	1.6	1.9

Note. Space group: *Pnma*. Atomic positions: Y: 4c (x, 0.25, z); Cr: 4b (0, 0, 0.5); O(1): 4c (x, 0.25, z) and O(2): 8d (x, y, z).

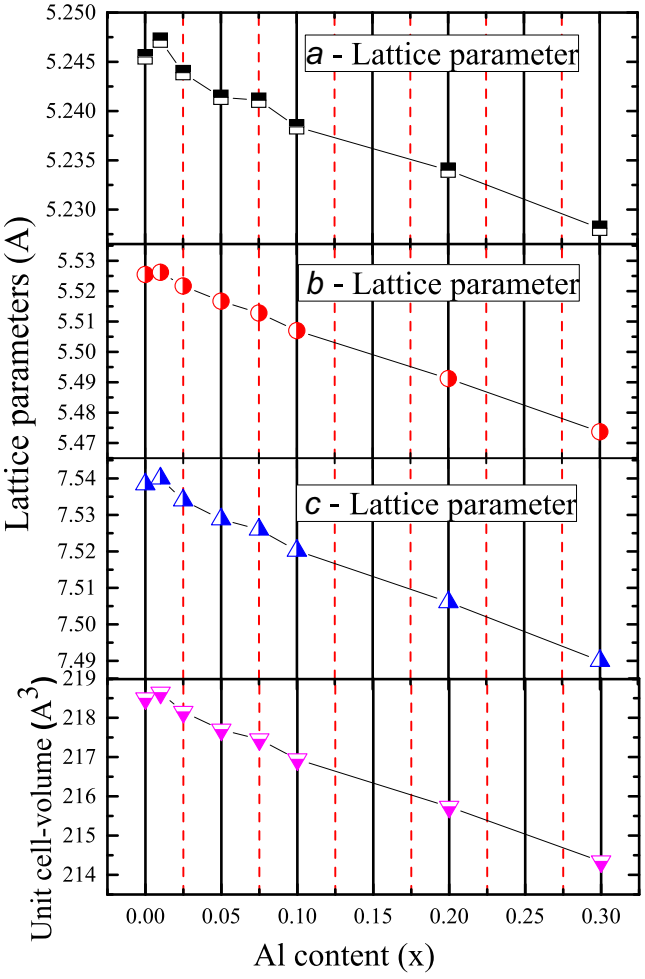

Fig. 2. Lattice parameters and unit-cell volume as a function of the Al content in the $YCr_{1-x}Al_xCrO_3$ compound.

we should note that the compressive effect by Al substitution increases the tilting along the c-axis ([001]-direction), while, on the other hand, the tilting angle along the *ab*-plane ([110] direction) decreases. Thus, the continuous deviation of the *Cr(1)–O–Cr(1)* bond angles and the octahedral distortion with Cr/Al substitution should produce a strong influence on the magnetic properties as will be discussed in what follows.

To determine the valence state of the ions in the $Y(Cr_{1-x}Al_x)O_3$ structure, we studied the core level (CL) by X-ray photoelectron spectroscopy (XPS). Fig. 3 shows the XPS survey spectra from 0 to 700 eV after Ar^+ etching the polycrystalline surface. The core level associated with Y^{3+}, Cr^{3+}, Al^{3+}, and O^{2-} elements are identified in their respective binding energy.

Fig. 4 shows the high-resolution spectra for the Al 2*s* and Cr 2*p* CL. The Cr $2p_{3/2}$ and Cr $2p_{1/2}$CL are localized at 576.22 eV and 585.62 eV, respectively. These values are consistent with the reported for Cr_2O_3 in the NIST XPS database: Cr $2p_{3/2}$: 576.0 eV–577.1 eV, average: 576.55 eV. On the other hand, at 118.58 eV is localized the Al 2s CL; this value is within the values range reported for Al_2O_3 in the NIST XPS database ref.: Al 2s: 116.25 eV–119.2 eV, average: 117.72 eV. The results showed here infer that the ions are in valence Cr^{3+} and Al^{3+}, respectively. Note also that the intensity of the Cr 2*p* CL decreases while the Al 2*s* CL increases with increasing Al content. The result is consistent with the gradual decrease of the lattice parameters, which shows that the partial Al^{3+} substitution takes place without changes in the oxidation state of the Cr^{3+} ion (See Table 1). Fig. 5 shows the XPS valence band spectra for all samples (inset) compared with the theoretical electronic density of states (DOS) of $YCrO_3$, which was determined from the band structure calculations. As expected, is observed a good correspondence between XPS valence band and DOS. As we can see there, the main contributions between −7.0 eV and 0.00 eV are Y 3*d*, Cr 3*d*, and O2*p* sates [24]. The bands close to Fermi level are of particular importance since they are responsible for the transport properties. In this case, the Cr 3d states localized between 0 and −0.8 eV contribute to the Fermi Level. The XPS valence band spectra show a peak decreasing in the intensity of the Cr 3d states near $N(E_F)$ as Al content increases as seen in the expanded scale in the inset of Fig. 5. This fact means that the DOS population at the Fermi level, in particular, the component Cr 3*d* localized near $N(E_F)$ decreases. This fact suggests changes in the transport properties as Al content is increased in the $YCrO_3$ matrix. To investigate the effect of the Al substitution on the transport properties, we calculated the electrical AC conductivity at room temperature from the capacitance and loss tangent data for each frequency (ω_i), according to the following formula;

$$\sigma_{\omega i}(T) = \frac{l}{s} \cdot \omega_i \cdot Cp_{\omega_i}(T) \cdot \tan \delta_{\omega_i}$$

Table 2
Geometrical parameters characterizing the crystal structure of $YCr_{1-x}Al_xO_3$ system. The octahedral distortion parameter Δ of a coordination polyhedron BO_N with an average bond length B–O ⟨d⟩, is defined as $\Delta = (1/N)\Sigma_{n=1,N}\{(d_n - \langle d\rangle)/\langle d\rangle\}^2$. The tilt angles φ and θ of CrO_6 octahedral around pseudocubic [0 0 1] and [1 1 0] direction are obtained from the two angles; θ_1 and θ_2 [Ref. [23]].

x =	0.000	0.010	0.025	0.050	0.075	0.100	0.200	0.300
Cr–O1:2	1.956(3)	1.956(2)	1.955(3)	1.952(2)	1.951(2)	1.949(3)	1.944(2)	1.939(2)
Cr–O2:2	1.897(3)	1.898(3)	1.892(2)	1.891(3)	1.889(3)	1.888(3)	1.884(3)	1.879(3)
Cr–O2:2	2.059(2)	2.059(3)	2.061(3)	2.059(3)	2.058(3)	2.057(2)	2.054(2)	2.049(2)
⟨Cr–O⟩	1.971	1.971	1.969	1.967	1.966	1.965	1.961	1.956
Δ(Cr–O) × 10^{-3}	2.31	2.31	2.51	2.53	2.52	2.54	2.57	2.61
Cr–O(1)–Cr	148.99(2)	148.99(2)	149.10(3)	149.37(2)	149.36(2)	149.47(3)	149.72(2)	149.81(2)
Cr–O(2)–Cr	148.67(1)	148.67(3)	148.83(2)	148.83(3)	148.83(3)	148.83(2)	148.82(2)	148.82(3)
⟨θ⟩	15.51	15.51	15.45	15.32	15.32	15.27	15.14	15.10
⟨ϕ⟩	10.88	10.88	10.86	10.67	10.67	10.59	10.41	10.34

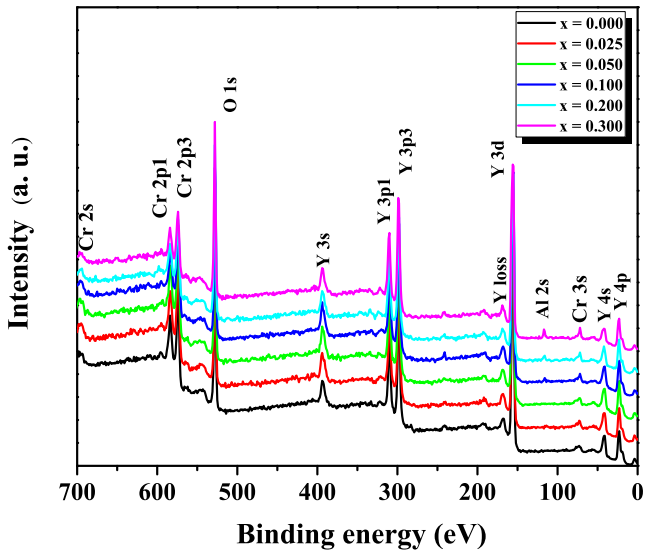

Fig. 3. XPS survey spectra of $YCr_{1-x}Al_xCrO_3$ polycrystalline samples.

where *l* and *s* are the thickness and the area of the electrode deposited on the sample, respectively. Electrical conductivity as a function of Al content at room temperature is shown in Fig. 6. There, it is observed a drastic decrease of the electrical conductivity from 2.8E−3 for x = 0 to 3.65E−4 for x = 0.01 and 3.44E−5 S.m^{-1} for x = 0.075 measured at room temperature and 100 kHz. After that, the electrical conductivity remains more and less constant taken the value of about 3.2E−5 for x = 0.3 of Al content. If we see with details the inset of Fig. 6, the XPS valence band spectrum for x = 0.075, 0.10 and 0.20 do not change significantly, which can explain the plateau observed in the electrical conductivity of these Al composition. However, the electrical conductivity shows an inconsistent since the electrical conductivity increases slightly for x = 0.3 sample. Reports have shown that the electronic properties of $YCrO_3$ change with the replacement total of Cr ions by Al ions; for example, it is observed an increase in the band gap of 1.43 eV for $YCrO_3$ to 7.1 eV for $YAlO_3$ [Refs. 18,25], respectively. As a consequence, a change in the conductivity is reported, for the undoped $YAlO_3$ is about 2.5 E−6 S.cm^{-1} at 800 °C [Ref. 26,27]; while, for $YCrO_3$ is 2.8E−3 S.cm^{-1} at room temperature. However, details permittivity studies are in progress to understand the effect of the Al substitution on the current density and polar behavior.

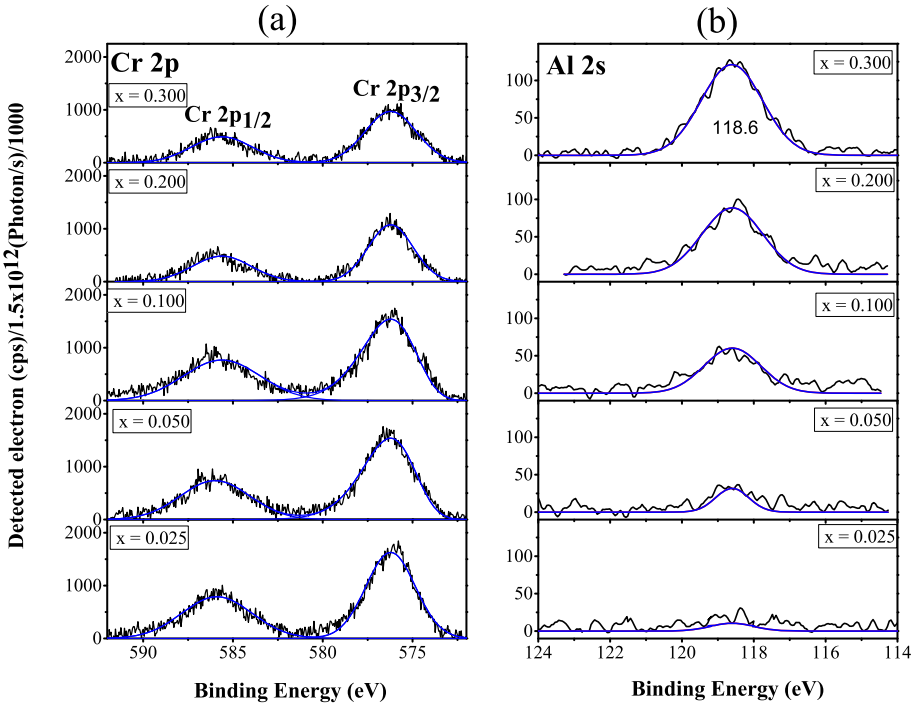

Fig. 4. (a) High-resolution XPS spectra of the Cr 2p and (b) Al 2s of $YCr_{1-x}Al_xCrO_3$ polycrystalline samples.

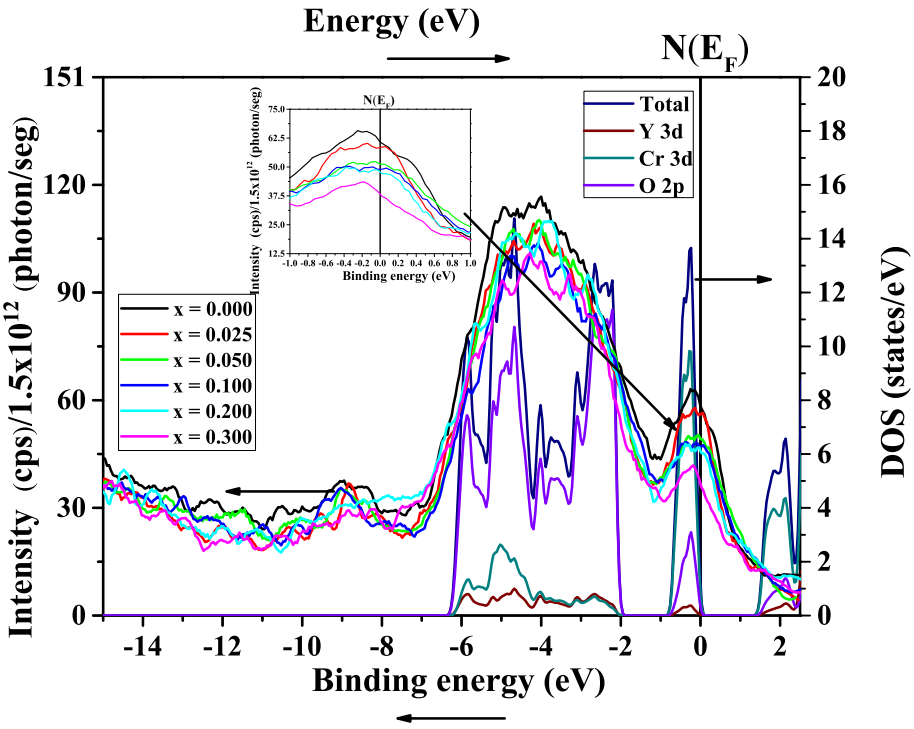

Fig. 5. Comparisons of XPS Valence band and electronic density of states for $YCr_{1-x}Al_xCrO_3$ polycrystalline samples. The scale on the right side corresponds to DOS and the left to XPS Valence band. The inset shows the zoom from −1.0 to 1.0 eV in the valence band.

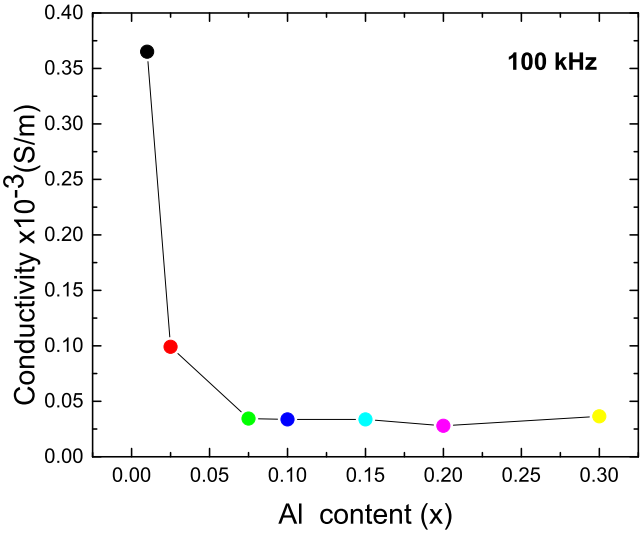

Fig. 6. Electrical conductivity for $YCr_{1-x}Al_xO_3$ at room temperature taken at 100 kHz.

The molar DC susceptibility from room temperature down to 2 K in the ZFC and FC mode is seen in Fig. 7a and b. For pristine sample, the ZFC curve shows a very weak magnetic signal at low temperature, which is monotonically increased with increasing temperature up to Néel temperature, T_N where a sudden drop of susceptibility occurs at 142 K. On the other hand, a typical ferromagnetic saturation curve is observed in the FC mode with a magnetization value of ~0.16 emu/mol at 2 K. The strong splitting of the ZFC and FC mode is an experimental observation of weak ferromagnetism associated with Dzyaloshinsky-Moriya antiferromagnetic (AFM) interaction between Cr^{3+}–Cr^{3+} ions [10,28]. Note that

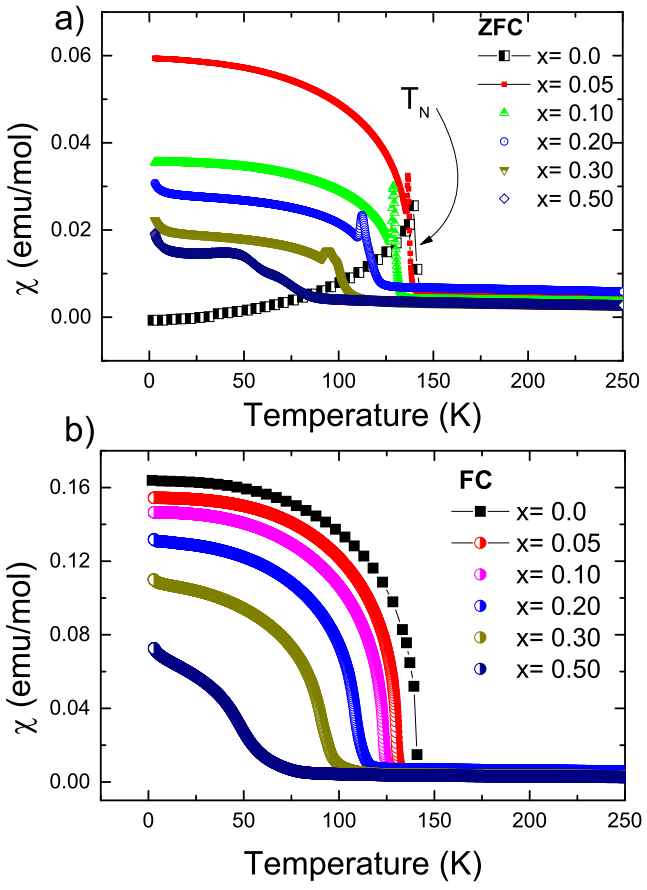

Fig. 7. The molar DC susceptibility of $YCr_{1-x}AlxO_3$ for $0 < x < 0.5$ in applied magnetic field of 1 kOe. (a) ZFC mode and (b) FC mode.

the Cr/Al substitution have strong effects in the magnetization curves. Thus, it is observed that i) T_N decreases to 129, 115, 100 and 65 K for x = 0.05, 0.1, 0.2, 0.3 and 0.5 composition. ii) The saturated susceptibility curves are restored in the ZFC mode, and the magnetic transition is broader with Al substitution. iii) The susceptibility value decreases from ~0.060 emu/mol for x = 0 to 0.019 emu/mol for x = 0.5 and from 0.16 for x = 0 to 0.072 emu/mol for x = 0.5 at 2 K in the ZFC and FC mode, respectively.

Fig. 8a and b show the magnetization versus applied magnetic field measured at 5 and 50 K. The pristine sample shows a typical hysteresis loop in agreements with the reported curves [10,29,30]. For clarity, Fig. 8c and d show the effect of the Al substitution on the coercive field, H_c and remnant magnetization, M_r at 5 and 50 K, respectively. It is observed that the H_c increases from 11.8 kOe for x = 0 to 18.9 kOe for x = 0.1 and then the H_c decreases monotonically to 3.5 kOe for x = 0.5 at 5 K. A similar behavior of H_c is observed at 50 K, where the H_c increases slightly for x = 0.05 and then decreases down to 1.41 kOe for x = 0.5 composition. On the other hand, the M_r does not show any anomaly as is seen in the H_c plot, but; it is observed that the M_r is almost the same for the x = 0.05 and 0.1 samples when both samples are warmed from 5 to 50 K (Fig. 8d). It is interesting to understand the role that Al^{3+} plays in the magnetic properties. As mentioned before, the dominant exchange interaction between the Cr^{3+}–Cr^{3+} ions give a G-type canted antiferromagnetic configuration due to D-M exchange interaction. It is well known that the T_N of $RCrO_3$ is strongly influenced by R ionic radii independently of the intrinsic magnetic moment of R ions. It is observed an increase of the tilting angle along the [001] direction from 10.3° for $LaCrO_3$ to 17.8° for $LuCrO_3$ producing a change in the T_N from ~285 to ~112 K, respectively [12]. One question that at once arises here is, whether the Al^{3+} substitution has the same effect on the octahedral tilting and, consequently, on the T_N in the same way as the rare earth substitution in the orthochromites. As mentioned before, the *Cr–O–Cr* angles along the [100] and [010] direction correspond to the anti-phase octahedral tilting $\alpha^- = \alpha^-$ and the angle along the [001] direction corresponds to the in-phase octahedral tilting, α^+. These octahedral tiltings occur in the basal *ab*-plane and along the *c*-direction, respectively. These values along with octahedral distortion are listed in Table 2. In $YCr_{1-x}Al_xO_3$, we observe a similar situation as is observed in the RCrO3 family since Al^{3+} substitution increase the tilt $\phi_{[001]}$ angle from 11.20 to 11.40 changing the T_N from 140 to 65 K. If we apply the earlier criterion, the T_N must decrease as is observed here. Thus, we can infer that the T_N decreasing is predominantly associated with the *Cr–O(2)–Cr* tilting angle in $YCr_{1-x}Al_xO_3$. In other words, the Al^{+3} substitution weakens DM interaction. To find a correlation between the tilting angles (ϕ, θ) and octahedral distortion (Δ) with the ferromagnetic parameters, H_c; we graph these parameters as a function of Al^{3+} content as seen in Fig. 9. A noticeable increase in the H_c is observed for x = 0.05 of Al as shown in Fig. 9d. Here, two types of mechanisms can be proposed to explain that: i) a geometrical deformation, which is tuned not only by the tilt angle along the [001] and [110] direction but also the octahedral distortion, Δ and ii) changes of electronic structure as a result of the Cr–Cr exchange interaction dilution by the nonmagnetic Al^{3+} ion. These two possibilities are discussed here. The first one can be observed in the Fig. 9 and is limited by the hatched bar, and it occurs for x < 0.05 of Al content. From this graph, we can infer that a strong local deformation can be appreciated by a sudden increase of the octahedral distortion and the angles around x = 0.05 composition. In this point, the maximum in H_c infers that the local deformation is pinning the ferromagnetic domains producing an increase of H_c. For x > 0.05 a competing effect between the local deformation and the dilution of the Cr–Cr exchange interaction by Al substitution begin to be dominant resulting in a monotonic decreasing of the ferromagnetic parameters. Thus, we can infer that the ferromagnetic decreases (H_c, M_r) for x > 0.05 should be ascribed to the change in the electronic structure. The XPS valence bands can corroborate this assertion, which is shown in the inset of Fig. 6. The

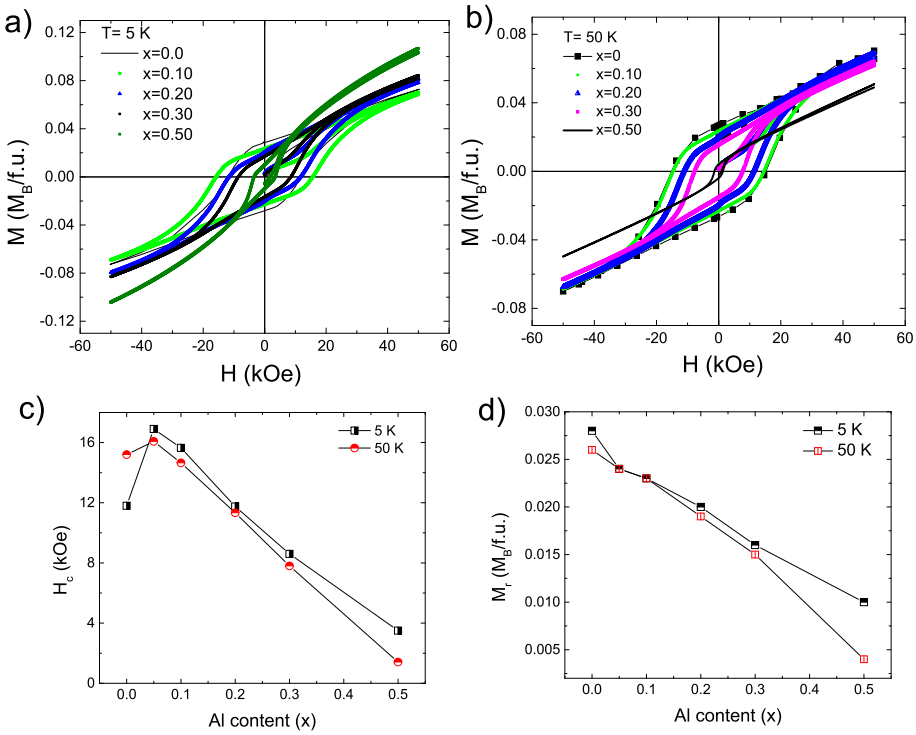

Fig. 8. (a, b) Magnetization as a function of the applied magnetic field at 5 and 50 K for $YCr_{1-x}Al_xO_3$ with 0 < x < 0.5 compositions. Graphs (c) and (d) show the H_c and M_r values as a function of Al content taken from magnetization curves at 5 and 50 K.

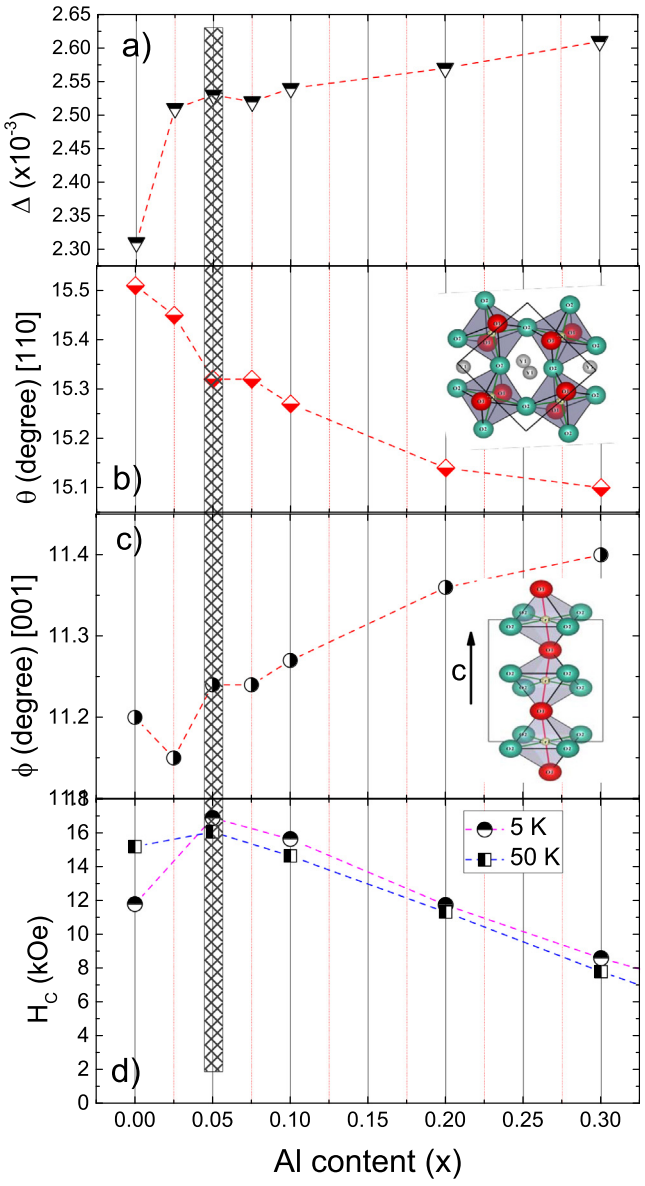

Fig. 9. The octahedral distortion (Δ), the tilting angles (ϕ, θ) and H_c parameters are compared and plotted as a function of Al content.

decrease of the XPS valence band at the Fermi energy infers the DOS population of the Cr 3d component at the Fermi level, decrease. Thus, we suppose that the electronic depopulation of the DOS at Fermi energy by the Al^{3+} substitution dilutes the dominant Cr–Cr exchange interaction being the main responsible for the decreasing of the ferromagnetic signal (low H_c and M_s) at 5 and 50 K beyond of x = 0.1 composition.

4. Conclusion

In this study, we presented a systematic study that begins with the synthesis, the structural details to finish with the electric and magnetic response of the $YCr_{1-x}Al_xO_3$ samples. It is observed that the lattice parameters and volume decrease with Al substitution. Also, the XPS high-resolution spectra for the Al 2s and Cr 2p window confirm 3+ oxidation state in the solid solution. The Al^{3+} substitution has notable effects on the electric and magnetic properties. It is found that the electrical conductivity shows a drastic decreasing for x < 0.075 of Al content after that the electrical conductivity remains constant. Furthermore, two mechanisms that tune the magnetic properties are discussed and proposed. The first one is related to the local deformation at low Al concentration (Al < 0.10), and the second, it is a consequence of the nonmagnetic Al^{3+} dilution. Local deformation influences the H_c since these local field deformations pinning the ferromagnetic domains, so increase the H_c for low Al^{3+} content. On the other hand, as Al^{3+} ions are introduced in the $YCrO_3$ matrix, the depopulation of Cr^{3+} ions, at the Fermi energy and the octahedral tilting decrease the magnetization and the T_N, respectively. This fact is confirmed by the decreasing of the intensity of the valence band contribution of the Cr^{3+} ion at the Fermi energy as is observed by XPS. Thus, it is found that not only the dilution of the Cr–Cr exchange interaction by the nonmagnetic Al^{3+} ion but also the tilting and the octahedral distortion tune the magnetic properties.

Acknowledgements

A. Durán thanks, PAPIIT-UNAM project IN103016. R.E. acknowledges the support of PAPIIT-UNAM project IN106116/28. Specials thanks to L. Huerta for the XPS technical support and the fruitful comments on the XPS analysis. The technical assistance for P. Casillas and A. Tejeda-Cruz is greatly acknowledged.

Appendix A. Supplementary data

Supplementary data associated with this article can be found, in the online version, at https://doi.org/10.1016/j.jmmm.2017.12.106.

References

[1] Y. Shen, M. Liu, T. He, S.P. Jiang, Preparation, electrical conductivity, and thermal expansion behavior of dense $Nd_{1-x}Ca_xCrO_3$ solid solutions, J. Am. Ceram. Soc. 92 (10) (2009) 2259–2264.
[2] S.B. Adler, M. Cassidy, P.A. Connor, J. Druce, T. Horita, J.T.S. Irvine, T. Ishihara, Z. Jaworski, et al., List of contributors, High-Temperature Solid Oxide Fuel Cells for the 21st Century, Elsevier, 2016.
[3] N.Q. Minh, Ceramic fuel cells, J. Am. Ceram. Soc. 76 (3) (1993) 563–588.
[4] J.R. Sahu, C.R. Serrao, N. Ray, U.V. Waghmare, C.N.R. Rao, Rare earth chromites: a new family of multiferroics, J. Mater. Chem. 17 (1) (2007) 42.
[5] K. Ramesha, A. Llobet, T. Proffen, C.R. Serrao, C.N.R. Rao, Observation of local non-centrosymmetry in weakly biferroic $YCrO_3$, J. Phys.: Condens. Matter 19 (10) (2007) 102202.
[6] A. Durán, A.M. Arévalo-López, E. Castillo-Martínez, M. García-Guaderrama, E. Moran, M.P. Cruz, F. Fernández, M.A. Alario-Franco, Magneto-thermal and dielectric properties of biferroic $YCrO_3$ prepared by combustion synthesis, J. Solid State Chem. 183 (8) (2010) 1863–1871.
[7] R. Ramesh, Ferroelectrics: a new spin on spintronics, Nat. Mater. 9 (5) (2010) 380–381.
[8] A.B.M. Bibes, Towards a magnetoelectric memory, Nat. Mater. 7 (2008) 425–426.
[9] M. Gajek, M. Bibes, S. Fusil, K. Bouzehouane, J. Fontcuberta, A. Barthélémy, A. Fert, Tunnel junctions with multiferroic barriers, Nat. Mater. 6 (4) (2007) 296–302.
[10] C.R. Serrao, A.K. Kundu, S.B. Krupanidhi, U.V. Waghmare, C.N.R. Rao, Biferroic $YCrO_3$, Phys. Rev. B 72 (22) (2005) 220101.
[11] E.F. Bertaut, Representation analysis of magnetic structures, Acta Crystallogr. Sect. A 24 (1) (1968) 217–231.
[12] J. Prado-Gonjal, R. Schmidt, J.J. Romero, D. Ávila, U. Amador, E. Morán, Microwave-assisted synthesis, microstructure, and physical properties of rare-earth chromites, Inorg. Chem. 52 (1) (2013) 313–320.
[13] B. Rajeswaran, P. Mandal, R. Saha, E. Suard, A. Sundaresan, C.N.R. Rao, Ferroelectricity induced by cations of nonequivalent spins disordered in the weakly ferromagnetic perovskites, $YCr_{1-x}M_xO_3$ (M = Fe or Mn), Chem. Mater. 24 (18) (2012) 3591–3595.
[14] V.G. Nair, A. Das, V. Subramanian, P.N. Santhosh, Magnetic structure and magnetodielectric effect of $YFe_{0.5}Cr_{0.5}O_3$, J. Appl. Phys. 113 (21) (2013) 213907.
[15] T. Bora, S. Ravi, Sign reversal of magnetization and tunable exchange bias field in $NdCr_{1-x}Fe_xO_3$ (x = 0.05–0.2), J. Magn. Magn. Mater. 386 (2015) 85–91.
[16] N. Sharma, B.K. Srivastava, A. Krishnamurthy, A.K. Nigam, Magnetic behaviour of the orthochromite $La_{0.5}Gd_{0.5}CrO_3$, Solid State Sci. 12 (8) (2010) 1464–1468.
[17] B. Rajeswaran, D.I. Khomskii, A.K. Zvezdin, C.N.R. Rao, A. Sundaresan, Field-induced polar order at the Néel temperature of chromium in rare-earth orthochromites: interplay of rare-earth and Cr magnetism, Phys. Rev. B 86 (21) (2012) 214409.

[18] D.M. Bercha, K.Z. Rushchanskii, M. Sznajder, A. Matkovskii, P. Potera, Elementary energy bands in ab initio calculations of the $YAlO_3$ and SbSI crystal band structure, Phys. Rev. B 66 (19) (2002) 195203.
[19] A. Altomare, M.C. Burla, C. Giacovazzo, A. Guagliardi, A.G.G. Moliterni, G. Polidori, R. Rizzi, Quanto: a Rietveld program for quantitative phase analysis of polycrystalline mixtures, J. Appl. Crystallogr. 34 (3) (2001) 392–397.
[20] A. Durán, C. Meza F, G.G.C. Arizaga, Hydroxide precursors to produce nanometric $YCrO_3$: characterization and conductivity analysis, Mater. Res. Bull. 47 (6) (2012) 1442–1447.
[21] R.D. Shannon, Revised effective ionic radii and systematic studies of interatomic distances in halides and chalcogenides, Acta Crystallogr. Sect. A 32 (5) (1976) 751–767.
[22] J.A. Alonso, M.J. Martínez-Lope, M.T. Casais, M.T. Fernández-Díaz, Evolution of the Jahn–Teller distortion of MnO_6 octahedra in $RMnO_3$ perovskites (R = Pr, Nd, Dy, Tb, Ho, Er, Y): a neutron diffraction study, Inorg. Chem. 39 (5) (2000) 917–923.
[23] Y. Zhao, D.J. Weidner, J.B. Parise, D.E. Cox, Critical phenomena and phase transition of perovskite – data for $NaMgF_3$ perovskite. Part II, Phys. Earth Planet. Inter. 76 (1-2) (1993) 17–34.
[24] R. Escamilla, L. Huerta, M. Romero, E. Verdin, A. Durán, Evidence of mixed valence Cr $$^{+3}$$ + 3/Cr $$^{+4}$$ + 4 in Y $$_{1−x}$$ 1 − xCa $$_x$$ x CrO $$_3$$ 3 polycrystalline ceramics by X-ray photoelectron spectroscopy, J. Mater. Sci. 52 (5) (2017) 2889–2894.
[25] Z. Huang, J. Feng, W. Pan, First-principles calculations of mechanical and thermodynamic properties of $YAlO_3$, Comput. Mater. Sci. 50 (10) (2011) 3056–3062.
[26] R. Hariharan, P. Gopalan, Chemical synthesis and characterization of Ca-substituted $YAlO_3$ as electrolyte for solid oxide fuel cells, J. Alloys Compd. 496 (1-2) (2010) 528–535.
[27] R. Hariharan, P. Gopalan, Effect of A-site substitution on electrical conductivity and microstructure of $YAlO_3$, J. Mater. Res. 27 (15) (2012) 2017–2023.
[28] I.A. Sergienko, E. Dagotto, Role of the Dzyaloshinskii-Moriya interaction in multiferroic perovskites, Phys. Rev. B 73 (2006) 094434.
[29] A. Durán, H. Tiznado, J.M. Romo-Herrera, D. Domínguez, R. Escudero, J.M. Siqueiros, Nanocomposite $YCrO_3/Al_2O_3$: characterization of the core-shell, magnetic properties, and enhancement of dielectric properties, Inorg. Chem. 53 (10) (2014) 4872–4880.
[30] A. Durán, E. Verdin, R. Escamilla, F. Morales, R. Escudero, Mechanism of small-polaron formation in the biferroic $YCrO_3$ doped with calcium, Mater. Chem. Phys. 133 (2-3) (2012) 1011–1017.